Resonators for accurate dielectric measurements in conducting liquids

Jean Hamelin, James B. Mehl,[a] and Michael R. Moldover[b]
National Institute of Standards and Technology, Physical and Chemical Properties Division, Gaithersburg, Maryland 20899

(Received 26 August 1997; accepted for publication 9 October 1997)

The compact, rugged, re-entrant radio-frequency resonator [A. R. H. Goodwin, J. B. Mehl, and M. R. Moldover, Rev Sci. Instrum. **67**, 4294 (1996)] was modified for accurate measurements of the zero-frequency dielectric constant (relative electric permittivity) ϵ_r of moderately conducting liquids such as impure water. The modified resonator has two modes with frequencies near $216/\sqrt{\epsilon_r}$ MHz and $566/\sqrt{\epsilon_r}$ MHz. The results for ϵ_r at both frequencies were consistent within $0.0002\epsilon_r$, verifying that the low-frequency limit had been attained with water samples with conductivities in the range 100–2500 μS/m. The results for water and for the insulating liquid cyclohexane were within $0.0005\epsilon_r$ of literature values. The present analysis is based on a simplified equivalent circuit that accounts for the loading of the resonator by the external instrumentation. This circuit can easily be generalized for a resonator with three or more modes. The present resonator has a thick gold plating on its interior surfaces. With the plating, the quality factors Q of the resonances varied in a predictable way with frequency and temperature. Predictable Qs were essential for obtaining accurate values of ϵ_r. [S0034-6748(98)03101-3]

I. INTRODUCTION

Recently, Goodwin *et al.*[1] presented techniques for fabricating and for using rugged, compact, re-entrant radio-frequency resonators to accomplish two tasks: (1) the automated detection of phase boundaries in dense fluid mixtures at high pressures; and (2) the measurement of dielectric constants (relative electric permittivity) ϵ_r of dilute gases to deduce dipole moments. The first task exploited the high sensitivity of the resonance frequency measurements to detect small changes in ϵ_r. However, this task did not require accurate values of ϵ_r. The second task required accurate values of ϵ_r; however, the accurate values of ϵ_r were needed only in the narrow range $1 \leqslant \epsilon_r \leqslant 1.01$, even for quite polar gases. Furthermore, the gases were good insulators. The present work solves the problems that we encountered when using re-entrant resonators to make accurate measurements of ϵ_r for liquid water.

For the present work, we required accurate values of ϵ_r at ''zero'' frequency throughout the wide range $1 \leqslant \epsilon_r \leqslant 100$. Furthermore, accuracy was required despite the moderate conductivity of the water. In order to meet these requirements, it was necessary to model the resonator throughout the frequency range $0.1 \leqslant f_\alpha^w/f_\alpha^0 \leqslant 1$ and to verify the model. [Here f_α^0 are the resonance frequencies of the evacuated resonator and f_α^w are the resonance frequencies of the water-filled resonator; α is a mode index which indicates the high (h) and low (l) modes.]

The requirement for verifying a model led us to use the two-mode resonator shown in cross section in Fig. 1. The two modes of this resonator had frequencies in the ratio 2.62:1 that were near $216/\sqrt{\epsilon_r}$ MHz and $566/\sqrt{\epsilon_r}$ MHz. The results for water in the range $49 \leqslant \epsilon_r \leqslant 89$ for both modes were consistent within $0.0002\epsilon_r$, verifying that the low-frequency limit had been attained for water samples. (A detailed description of the water data will be published elsewhere.[2]) The water samples had conductivities in the range 100–2500 μS/m. Near ambient temperature, the results for water and the results for the insulating liquid cyclohexane agree with published results within the uncertainty of the published results.

The resonance frequency data were analyzed with the simple lumped-component equivalent circuit shown in Fig. 1. This circuit accounts for the loading of the resonator by the external instrumentation. Furthermore, this circuit can easily be generalized for a resonator with three or more modes. Measurements of the resonance frequencies f_α^0 and quality factors Q of the evacuated resonator were used to determine combinations of component values for the equivalent circuit. Careful measurements of the resonator's dimensions were not required. The resonator's dilation with pressure was accounted for by measuring f_α^0 in helium as a function of pressure and correcting the results for the small dielectric polarizability of helium.

In essence, the resonator method for determining ϵ_r is to measure f_α^0 and f_α^w and to use the relation

$$\epsilon_r = (f_\alpha^0/f_\alpha^w)^2. \tag{1}$$

Equation (1) would be exact if the spatial distribution of the electric and magnetic fields within the resonator were identical in the empty and filled configurations. The most important correction to Eq. (1) results from the penetration of the magnetic field into the metal surfaces bounding the resonator. The penetration depth δ equals $1/\sqrt{\pi f \mu' \sigma'}$, where μ' and σ' are the magnetic permeability and conductivity of the metal surface, respectively. The penetration contributes an amount $g_{s\alpha}$ to the resonance half-width g_α, and decreases the resonance frequencies by an equal amount. For the resonator shown, after gold plating, with $\mu' \approx \mu_0$ and $\sigma \approx 4.6$

[a]Also at: Department of Physics and Astronomy, University of Delaware, Newark, DE 19716-2570.
[b]Electronic mail: michael.moldover@nist.gov

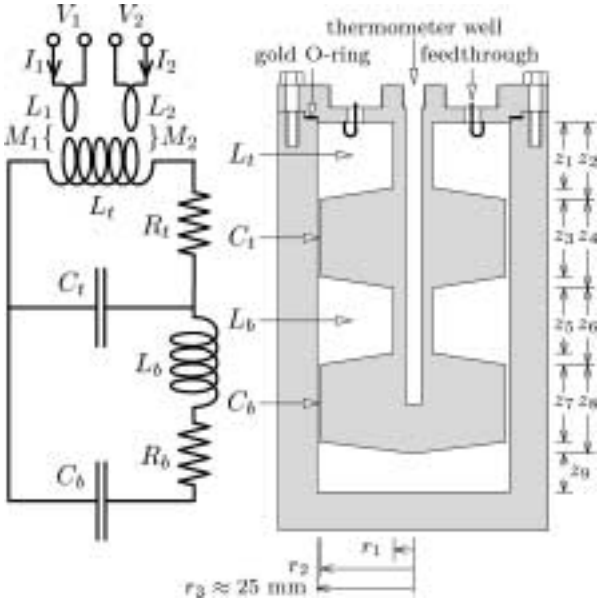

FIG. 1. Two-mode re-entrant radio-frequency resonator and equivalent circuit. The dimensions z_1 through z_9, and r_1 through r_3, in mm, are 17.19, 20.07, 20.12, 23.15, 16.98, 19.87, 19.99, 23.01, and 10.7; 5.015, 23.98, and 24.95. Approximate (vacuum) values of the components are $L_t = 5.88$ nH, $C_t = 33.5$ pF, $L_b = 6.19$ nH, $C_b = 35.2$ pF, $M_1 = M_2 = 0.17$ nH, and $L_1 = L_2 = 9.6$ nH. The effective resistances are approximately 0.008 Ω for the lower-frequency mode and 0.0058 Ω for the higher-frequency mode.

$\times 10^7$ S/m, the penetration depths are $\delta_h \approx 3\sqrt[4]{\epsilon_r}$ μm and $\delta_l \approx 5\sqrt[4]{\epsilon_r}$ μm. The fractional corrections to Eq. (1) are on the order of

$$g_{s\alpha}/f_\alpha \sim \delta_\alpha/\ell \sim 0.001, \tag{2}$$

where ℓ is a characteristic apparatus dimension. The variation of $g_{s\alpha}/f_\alpha$ with ϵ_r is also on the order of 0.001. Thus, in contrast with Ref. 1, it was necessary to account carefully for the frequency dependence of δ_α. Careful accounting could not be done with a stainless-steel surface because the values of μ' for stainless steels differ significantly from the vacuum permeability μ_0 and they vary with temperature and heat treatment in a complex way. Thus, the stainless-steel resonator was plated with gold to a nominal thickness of 30 μm, which exceeded δ by a factor of 2 or more.

II. APPARATUS

A cross section of the two-mode resonator is shown in Fig. 1. The experimental procedures used with this apparatus are similar to those described in a recent paper on a single-mode re-entrant resonator.[1] Unnecessary details are not repeated in this article.

The resonator was machined from two pieces of 316 stainless steel, sealed with a gold *O* ring and bolted together as shown. Fill and drain connections (not shown) through the top and bottom pieces were used to fill and drain fluid samples and to evacuate the resonator.

The outer cylinder was immersed in a stirred-fluid bath which was regulated within 0.01 K. The bath temperature was measured with a platinum resistance thermometer calibrated on the ITS-90 scale and was located in a blind hole drilled deep into the center of the cavity lid (see Fig. 1). The uncertainty in the sample temperatures is approximately 0.01 K. The pressure was measured with a quartz pressure transducer which was isolated from the fluid sample by a stainless-steel bellows. The uncertainty in pressure measurements over the range 0–300 kPa is 0.05 kPa.

Electrical connections were provided through rigid coaxial lines supported by compression fittings which screwed into the top piece. The center conductors of the coaxial cables were welded to insulated feedthroughs whose extensions formed coupling loops. The feedthroughs were gold-plated Kovar, insulated with glass. As mentioned above, the inner surface of the resonator was electroplated with gold to a nominal thickness of 30 μm.

Resonances were detected by using a vector analyzer to measure the scattering parameter $\mathbf{S}_{21}$, defined (for properly terminated lines) as the complex ratio of voltage transmitted through the resonator to the voltage incident on the resonator. For a typical measurement, $\mathbf{S}_{21}$ was measured at 51 frequencies spanning $f_\alpha \pm 2g_\alpha$. A single-mode response function was fit to each data set to obtain precise values of f_α and g_α. A theoretical model of the experiment is required to obtain ϵ_r from these data.

III. A SIMPLE MODEL

A simple model contains the essential characteristics required to analyze data and determine dielectric properties. Consider a series of *LRC* circuit immersed in a fluid of relative electrical permittivity $\epsilon' - i\epsilon''$ and conductivity σ. The impedance of the capacitor is

$$\mathbf{Z}_c = \frac{1}{[i\omega(\epsilon' - i\epsilon'') + \sigma/\epsilon_0]C} = \frac{1}{i\omega\boldsymbol{\epsilon}_r C}, \tag{3}$$

where C is the capacitance without a fluid present. The combination

$$\boldsymbol{\epsilon}_r \equiv \epsilon' - i\epsilon'' - i\sigma/(\omega\epsilon_0) \tag{4}$$

will be used for brevity in the following. In general, the relative permittivity is complex, as expressed, e.g., by the Debye relaxation model. The equation shows that the effects of ϵ'' and conductivity are similar; however, the two terms may have different frequency dependences.

The impedance of an inductive section of an electromagnetic resonator has the form

$$\mathbf{Z}_l = i\omega L + (1+i)R, \tag{5}$$

where L is the inductance without a fluid present and R is a frequency-dependent resistance associated with current flow within the boundary layer of the metal resonator surfaces. (In principle, the inductance should be multiplied by the relative magnetic permeability μ_r of the fluid. For diamagnetic liquids such as water, μ_r differs from 1 by less than 10^{-5}.) The dimensions of the current-carrying region are a path length ℓ and a cross-sectional area $\ell'\delta$, where ℓ and ℓ' are lengths on the order of apparatus dimensions. The resistance (R) will be of order $\ell/(\ell'\sigma'\delta) \propto \sqrt{\omega/\sigma'}$.

The resonance condition is the vanishing of the series impedance $\mathbf{Z}_l + \mathbf{Z}_c$, which will occur at the complex resonance frequency $\mathbf{F} = f + ig$ related to $\boldsymbol{\epsilon}_r$ by

$$\epsilon_r = \frac{1+(-1+i)\omega RC\epsilon_r}{(2\pi \mathbf{F})^2 LC}. \tag{6}$$

The ratio $2g/f$ is usually expressed as $1/Q$, where Q is the quality factor of the resonance. For vacuum measurements the quality factor of the *LRC* circuit is determined by the surface resistivity

$$1/Q_s^0 = \omega RC. \tag{7}$$

The product LC depends on the apparatus dimensions and hence has weak pressure and temperature dependences. It was determined from measurements of $\mathbf{F}^0$ in helium at the experimental temperature and pressure, and corrected for the small polarizability of helium.

A working equation for data analysis can be obtained by expressing LC in terms of $\mathbf{F}^0$ and Q_s^0, and by expression $1/Q_s$ for the sample as the product of the vacuum value and a scaling factor proportional to $f^{3/2}\epsilon_r$:

$$\epsilon_r = \left(\frac{\mathbf{F}^0}{\mathbf{F}}\right)^2 \frac{1+(-1+i)(f/f^0)^{3/2}\epsilon_r/Q_s^0}{1+(-1+i)/Q_s^0}. \tag{8}$$

Equation (8) is a simple and effective working equation for determination of the complex parameter ϵ_r from measurements of $\mathbf{F}$. If the effects of coupling to the external circuit were sufficiently weak, Eq. (8) would suffice for data analysis. Unfortunately, coupling could not be neglected in these measurements. A more detailed circuit model was required. The detailed model shows how the external coupling could be made sufficiently weak so as to be negligible in future applications.

IV. A MORE COMPLETE MODEL

A. Equivalent circuit

The resonator consists of four annular sections. The circuit can be analyzed with a coupled coaxial waveguide model similar to the one used to describe the single mode resonator.[1] Such a model is useful for relating the resonance frequencies to the resonator dimensions because the effects of finite wavelength are taken into account. A simpler, lumped-component model, suffices for the analysis of the measurements reported here.

To a very good approximation, the two narrow-gap coaxial sections are capacitors, and the two wide-gap sections are inductors. The waveguide model[1] demonstrated that surface-conductivity effects are negligible in the capacitive sections but are important in the inductive sections. An equivalent circuit with the essential features is shown in Fig. 1. The inductance L_t of the top coaxial section is associated with current flow which encircles this section. The total impedance of the top inductive section, $i\omega L_t + (1+i)R_t$, includes a dissipative component associated with the current path, and a correction to the inductance associated with the additional magnetic field penetrating the metal walls. The top inductor is directly coupled to the top capacitor C_t. This capacitor is also coupled through an inductive path to the bottom capacitor C_b. Formulas for the capacitances, inductances, and resistances can be found in Ref. 1. The inductances and resistances listed in the caption to Fig. 1 were calculated from the dimensions of the apparatus. The capacitances listed in the caption could not be calculated with high accuracy because the widths of the narrow gaps were not well known. Instead, the capacitances were calculated from the measured vacuum resonance frequencies using the circuit model and the calculated inductances. The values so determined, when corrected for the fringing fields at junctions between the capacitive and inductive sections, are consistent with values estimated from the apparatus dimensions.[3]

The resonator is coupled to external coaxial cables with the small coupling loops shown in Fig. 1. The loops are formed of gold-plated wire of diameter 0.66 mm formed into U shapes with semicircular portions of mean diameter 5.0 mm and straight sections 2.6 mm long. One straight section of each loop is grounded to the top plate, the other is an extension of the central conductor of a coaxial line. The estimated self-inductance of the loops is $L_j \approx 6$ nH; the estimated mutual inductance M_j between loop j and inductor L_t is $0.22 \sin\theta_j$ nH, where θ_j is the angle between the plane of the loop and the field lines.

Reflections and transmissions of signals on lines coupling external instruments to two-port devices can be described in terms of a scattering matrix.[4] The parameter $\mathbf{S}_{21}$, which equals the ratio of the transmitted voltage amplitude to the incident voltage amplitude on properly terminated lines, calculated for the circuit of Fig. 1, is

$$\mathbf{S}_{21} = \frac{2R_0}{\mathbf{Z}^*} \frac{\omega M_1}{R_0 + i\omega L_1} \frac{\omega M_2}{R_0 + i\omega L_2}, \tag{9}$$

where

$$\mathbf{Z}^* = i\omega L_t + (1+i)R_t + \mathbf{Z}_\parallel + \mathbf{Z}_e,$$

$$\mathbf{Z}_\parallel = \frac{\mathbf{Z}_b}{1 + i\omega\epsilon_r C_t \mathbf{Z}_b},$$

$$\mathbf{Z}_b = \frac{1}{i\omega\epsilon_r C_b} + i\omega L_b + (1+i)R_b,$$

$$\mathbf{Z}_e = \frac{\omega^2 M_1^2}{R_0 + i\omega L_1} + \frac{\omega^2 M_2^2}{R_0 + i\omega L_2} = R_e + i\omega L_e.$$

Here $\mathbf{Z}_\parallel$ is the parallel equivalent impedance of C_t and $\mathbf{Z}_b$, and $\mathbf{Z}_e$ is the external impedance coupled through the loops.

B. Resonance line shape

Equation (9) predicts a resonance line shape with complex resonance frequencies $\mathbf{F}_\alpha$ at the zeroes of $\mathbf{Z}^*$. An expansion of the response function about $\mathbf{F}_\alpha$ has the form

$$\mathbf{S}_{21}(f) = \frac{\mathbf{A}f}{f^2 - \mathbf{F}_\alpha^2} + \mathbf{B} + \mathbf{C}(f - \tilde{f}), \tag{10}$$

where $\tilde{f}$ is any fixed frequency near f_α. This expansion was used to determine the complex resonance frequencies $\mathbf{F}_\alpha$. Its use in the present application was validated by tests with synthetic data generated using Eq. (9). Equation (10) was then fit to the synthesized data and the resonance frequencies determined in the fit were compared with the parameters used in the synthesis. The fits were found to underestimate the real part of $\mathbf{F}_\alpha$ by a small fractional amount equal to

$1/(8Q^2)$. This correction, although negligible for the results reported in this article, was routinely made in our analysis of data over the wider temperature range.

C. Resonance frequencies

The resonance condition $\mathbf{Z}^*=0$ is, with $x=\omega^2$,

$$(1+\boldsymbol{\nu}_1-\boldsymbol{\epsilon}_r x/x_1)(1+\alpha+\boldsymbol{\nu}_2-\boldsymbol{\epsilon}_r x/x_2)=\alpha, \tag{11}$$

where

$$x_1=1/[(L_t+L_e)C_t],$$

$$x_2=1/(L_bC_b),$$

$$\alpha=C_b/C_t,$$

$$\boldsymbol{\nu}_1=[(-1+i)R_t+iR_e]\omega C_t\boldsymbol{\epsilon}_r,$$

$$\boldsymbol{\nu}_2=(-1+i)\omega R_bC_b\boldsymbol{\epsilon}_r.$$

If the weak frequency dependences of R_e, L_e, and the $\boldsymbol{\nu}_j$ are neglected, Eq. (11) can be solved formally using the quadratic formula. An approximate solution for the complex resonance frequency $\mathbf{F}_\alpha=f_\alpha+ig_\alpha=\sqrt{x}/2\pi$, valid for small $|\boldsymbol{\nu}_j|$, is

$$\mathbf{F}_\alpha^2\boldsymbol{\epsilon}_r\approx F_{\alpha,0}^2[1+A_\alpha\boldsymbol{\nu}_1+B_\alpha\boldsymbol{\nu}_2], \tag{12}$$

where

$$F_{\alpha,0}^2=\frac{y_1\pm y_2}{8\pi},$$

$$A_\alpha=\frac{x_1(1\pm y_3/y_2)}{y_1\pm y_2}\approx\begin{cases}0.120\\1.93\end{cases},$$

$$B_\alpha=\frac{x_2(1\mp y_3/y_2)}{y_1\pm y_2}\approx\begin{cases}0.254\\0.746\end{cases},$$

$$y_1=x_1+(1+\alpha)x_2,$$

$$y_2=\sqrt{y_1^2-4x_1x_2},$$

$$y_3=x_1-(1+\alpha)x_2.$$

(The numerical values correspond to the component values in the caption to Fig. 1.)

Equation (12) displays the dependence of the resonance frequencies and half-widths on the small quantities $\boldsymbol{\nu}_j$, which depend on the surface resistivity and the coupled external impedance. It is convenient to also separate off the dependence on the external inductance L_e which is implicit in $F_{\alpha,0}$ in the form of a series expansion

$$F_{\alpha,0}^2\approx f_{\alpha,0}^2[1+D_\alpha], \tag{13}$$

where $f_{\alpha,0}$ is $F_{\alpha,0}$ evaluated with $L_e=0$, and

$$D_\alpha=\frac{x_1}{y_2}\frac{y_2\pm(y_1-2x_2)}{y_1\pm y_2}\frac{L_e}{L_t}\approx\frac{L_e}{L_t}\begin{cases}0.30\\0.70\end{cases}.$$

A resonance condition similar to Eq. (6) can now be formed

$$(f_\alpha+ig_\alpha)^2\boldsymbol{\epsilon}_r=f_{\alpha,0}^2\left[1+\frac{-1+i}{Q_s}+\frac{i}{Q_e}+D_\alpha\right], \tag{14}$$

where

$$1/Q_s=\omega_\alpha(A_\alpha R_tC_t+B_\alpha R_bC_b)\boldsymbol{\epsilon}_r$$

and

$$1/Q_e=\omega_\alpha A_\alpha R_eC_t\boldsymbol{\epsilon}_r.$$

A modified working equation for data analysis based on Eq. (14) is

$$\boldsymbol{\epsilon}_r=\left(\frac{\mathbf{F}_\alpha^0}{\mathbf{F}_\alpha}\right)^2\frac{1+\dfrac{-1+i}{Q_s^0}\left(\dfrac{f_\alpha}{f_\alpha^0}\right)^{3/2}\boldsymbol{\epsilon}_r+\dfrac{i}{Q_e}+D_\alpha}{1+\dfrac{-1+i}{Q_s^0}+\dfrac{i}{Q_e^0}+D_\alpha^0}. \tag{15}$$

The form is chosen so that quantities which can be determined directly through experiment are explicit, and so that the dependence on the model and apparatus dimensions is limited to those terms which cannot be evaluated otherwise. The magnitudes of the various terms at 293 K are as follows. The surface term $1/Q_s^0$ equals 3.8×10^{-4} for the higher-frequency mode and 6.3×10^{-4} for the lower-frequency mode. The corresponding values in the numerator are scaled by a factor $(f_\alpha/f_\alpha^0)^{3/2}\boldsymbol{\epsilon}_r\approx\sqrt[4]{\boldsymbol{\epsilon}'}$.

For the extreme case of water, the scaling factor is approximately 3 so the total effect of $1/Q_s$ on the determination of $\boldsymbol{\epsilon}_r$ with the lower-frequency mode will be no greater than 0.2%. The effects of external coupling in Eq. (15) appear in two terms. The term $1/Q_e^0$, for vacuum measurements at 293 K, equals 1.3×10^{-4} for the higher-frequency mode and 1.5×10^{-4} for the lower-frequency mode. This term is purely dissipative for real $\boldsymbol{\epsilon}_r$. Its magnitude decreases rapidly with frequency and is only about 2×10^{-5} for water, for both modes. For vacuum measurements the second external term has the values $D_h\approx75\times10^{-6}$ and $D_l\approx32\times10^{-6}$. Both values are less than 2×10^{-6} for measurements in water.

V. MEASUREMENTS AND ANALYSIS

A. Quality factors of evacuated resonator

For fluids with real $\boldsymbol{\epsilon}_r$, the inverse quality factor $1/Q$ is the sum of the surface-resistivity and the external contributions. As a check on the model, we measured the dependence of $1/Q$ on the orientation of the coupling loops. The loops were successively oriented at a series of angles $\theta_1\approx\theta_2$ with respect to the field lines in the upper inductor. For identical coupling loops, the external impedance is proportional to $M_1^2=M_{10}^2\sin^2\theta_1$. For each mode, $1/Q$ was found to be approximately linear in $\sin^2\theta_1$, with slopes 0.27 ± 0.02 for the higher-frequency mode and 0.33 ± 0.04 for the lower-frequency mode. (The uncertainties here are one standard error, as estimated from the linear fits.) The maximum mutual inductance calculated from the slopes is $M_{10}=(0.22\pm0.01)$ nH, in excellent agreement with the value estimated from the loop dimensions. The self-inductance calculated from the slopes is $L_1\approx(7.8\pm1.4)$ nH. The higher uncertainty of the latter value can be traced to the smallness of $(\omega L_1/R_0)^2<0.3$ in these measurements.

In preliminary measurements, $1/Q_s$ was larger than the value calculated using the resistivity of gold.[5] Additional gold was applied until the estimated thickness exceeded 30 μm. The coupling loops were then set at $\theta_1\approx\theta_2\approx45°$, and

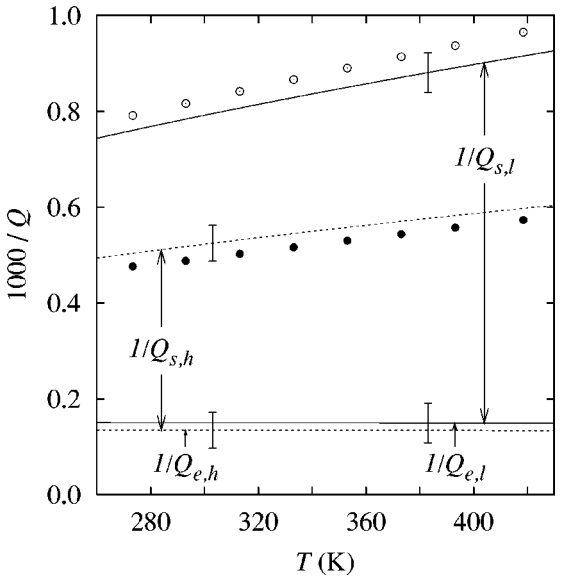

FIG. 2. Surface ($1/Q_s$) and external ($1/Q_e$) contributions to $1/Q$, and measurements of $1/Q$ in vacuum. Lower frequency mode: (○), measurements; (—), calculated. Higher frequency mode: (●), measurements; (---), calculated. The error in $1/Q_e$ is systematic. The error brackets represent ± 2 standard uncertainties. Literature values of the resistivity of gold were used to calculate $1/Q_s$. Uncertainties in the measured values of $1/Q$ are insignificant.

the Q was measured as a function of temperature between 270 and 420 K. The results, shown in Fig. 2, show good agreement between the calculated and measured values.

B. Uncertainties in determination of ϵ_r

Analysis of data taken in fluid samples to determine ϵ_r requires values of $1/Q_s$, which could be either calculated from the model or determined from scaled vacuum values. The effects of small inaccuracies in the model and uncertainties in the apparatus dimensions are minimized by using scaled vacuum values of $1/Q_s = 1/Q_{\text{expt}} - 1/Q_e$. The major uncertainty in this quantity is the uncertainty in $1/Q_e$. At 293 K the standard uncertainty $\Delta(1/Q_e)$ is $0.05/Q_s$ for the higher-frequency mode and $0.03/Q_s$ for the lower-frequency mode. The same fractional uncertainties apply to scaled values, provided that the gold plating is sufficiently thick. The contribution of the uncertainty in the external coupling to the standard fractional uncertainty of ϵ_r values obtained with Eq. (15) is approximately $0.05(\sqrt[4]{\epsilon'}-1)/Q_s^0 \approx 2\times10^{-5}(\sqrt[4]{\epsilon'}-1)$ for the higher-frequency mode and $0.03(\sqrt[4]{\epsilon'}-1)/Q_s^0 \approx 2\times10^{-5}(\sqrt[4]{\epsilon'}-1)$ for the lower-frequency mode. The uncertainty in the determination of the vacuum frequencies contributes an addition 1×10^{-5} to the standard fractional uncertainty of ϵ'.

C. Dielectric properties of cyclohexane

Measurements were made on a sample of spectrophotometric grade cyclohexane at three temperatures. Experimental values of ϵ' determined from the measurements are listed in Table I. The value of ϵ' determined with the higher-frequency mode is systematically 0.01% higher than the value determined with the lower-frequency mode. Both values lie within 0.05% of recent literature values.[6–8]

TABLE I. Dielectric constant of cyclohexane at three temperatures near ambient conditions. The sample pressure was in the range 98.7–98.9 kPa.

	293.15 K	298.15 K	303.15 K
Low mode	2.0238	2.0160	2.0082
High mode	2.0240	2.0162	2.0084
Reference 6		2.01714	
Reference 7	2.0240		2.0119
Reference 8	2.0228	2.0150	2.0077

D. Dielectric properties of water

As reported elsewhere,[2] the apparatus was used to measure the dielectric properties of water over the temperature range 270–420 K. Room temperature results are reported here as an example.

Resonance frequencies were measured in two water samples at $T = 293.13$ K. The relative purity of the samples is indicated by measurements of its low-frequency conductivity using a commercial instrument which measured the conductivity at 290 Hz. The conductivities determined with this instrument are 109 μS/m for sample A and 30 μS/m for sample B. The measurements were taken at $p = 100$ kPa. Equation (14) was used to determine the complex permittivity of the sample from the measured resonance frequencies in water. The real part ϵ' is listed in Table II, together with values of the conductivity determined in the experiment as described below. For sample A, the two measurements of ϵ' differ by only 0.004%. For sample B, the difference is 0.014%.

Fernández *et al.*,[9] list the measurements of ten groups over the frequency range 100 Hz–1 MHz at $T = 298.14$ K. The mean and standard deviation of the ten measurements is 78.41 ± 0.08. The empirical function of Ellison *et al.*[10] was used to adjust this to to 80.21 ± 0.08, corresponding to our experimental temperature. Table II also lists values of ϵ' calculated from the empirical representation of Ellison *et al.*[10] and the value published by the International Union of Pure and Applied Chemistry.[11] Our four measurements, which have a mean and standard deviation of 80.203 ± 0.008, are in excellent agreement with the literature values.

The predicted fractional standard uncertainty in ϵ' traceable to the uncertainties in $1/Q_s$ and the vacuum frequencies is 4×10^{-5} for either mode, slightly smaller than the standard deviation of our four measurements. It is worth consid-

TABLE II. Dielectric permittivity ϵ' of water determined with the resonator at two frequencies, at $T = 293.13$ K and $p = 100$ kPa, and selected reference values.

f (MHz)	Sample A	Sample B
24.1	80.210	80.203
63.2	80.207	80.192
Average of above	80.203 ± 0.008	
Ref. 9 ($f < 1$ MHz)	80.21 ± 0.08	
Ref. 10	80.19 ± 0.03	
Ref. 11	80.17 ± 0.05	

TABLE III. Analysis of resonance dissipation for water samples. The conductivities determined at two widely different frequencies are in good agreement.

f (MHz)		Sample A	Sample B
24.1	$1000[\epsilon''+\sigma/(\epsilon_0\omega)]/\epsilon'$	7.76	2.70
	$1000\epsilon'/\epsilon''$	1.38	1.38
	σ (μS/m)	686	142
63.2	$1000[\epsilon''+\sigma/(\epsilon_0\omega)]/\epsilon'$	6.12	4.12
	$1000\epsilon'/\epsilon''$	3.64	3.64
	σ (μS/m)	700	137

ering whether additional uncertainty can be attributed to insufficient gold plating. The calculated penetration depths are in the ranges 9–10 μm for the higher-frequency mode and 15–16 μm for the lower-frequency mode. Both values are well below the estimated thickness of the gold plating (30 μm). Thus there should be sufficient gold for accurate calculation of the effects of surface resistivity.

The conductivity of the water samples was determined by assuming that the relaxation part of $\boldsymbol{\epsilon}_r$ could be modeled by a Debye form

$$\epsilon' - i\epsilon'' = \epsilon_\infty + \frac{\epsilon_s - \epsilon_\infty}{1 + i\omega\tau}. \tag{16}$$

Parameters recommended by Ellison *et al.*[10] were used in this equation to estimate the ratio $1/Q_{\text{relax}} = \epsilon''/\epsilon'$. The conductivity was then calculated from the experimental values of $\boldsymbol{\epsilon}_r$ using Eq. (4). The results are summarized in Table III. There is a significant uncertainty because of the need to subtract ϵ'', which varies from 18% to 88% of the total imaginary part of $\boldsymbol{\epsilon}_r$. Nevertheless there is good internal agreement between the values of the conductivity determined with the two modes. The average values, however, exceed the 290 Hz measurements with the conductivity meter by factors of 6.4 (sample A) and 4.6 (sample B). This may be a manifestation of the Maxwell–Wagner effect,[12] which predicts limiting constant conductivities at low and high frequencies.

VI. DISCUSSION

We have measured the real part of ϵ' for one cyclohexane and two water samples near room temperature. The measurements were made at two frequencies differing by a factor of 1:2.62. For each measurement, the two values of ϵ' differ by 0.01%. We believe that this difference is a good estimate of the uncertainty in the measurement.

In future applications we recommend reducing the external coupling to eliminate the associated uncertainties and taking precautions to ensure that the interior surface of the resonator is nonmagnetic and has a high conductivity.

[1] A. R. H. Goodwin, J. B. Mehl, and M. R. Moldover, Rev. Sci. Instrum. **67**, 4294 (1996).
[2] J. Hamelin, J. B. Mehl, and M. R. Moldover, Int. J. Thermophys. (submitted).
[3] The fringing capacitances can be estimated using the formalism of N. Macruwitz, *Waveguide Handbook* (McGraw–Hill, New York, 1951), Sec. 5.27. Vacuum values are 2.4 pF at junctions between the capacitive and inductive sections and 2.7 pF at the boundary between the bottom narrow-gap section and the cylindrical region at the bottom of the resonator. The capacitance C_b also includes a contribution of about 1.3 pF from this cylindrical region.
[4] See, e.g., R. E. Collin, *Foundations for Microwave Engineering* (McGraw–Hill, New York, 1992), Chap. 4.
[5] *Handbook of Modern Electronics and Electrical Engineering*, edited by C. Belove (Wiley, New York, 1986), Tables 7.1 and 7.7.
[6] H. T. French, M. Koshla, and K. N. Marsh, J. Chem. Phys. **20**, 1175 (1988).
[7] M. Claudius, Diploma work, Meresburg, 1975, cited in *Landolt-Börstein, Numerical Data and Functional Relationships in Science and Technology*, New Series, edited by O. Madelung (Springer, New York, 1991), Group IV, Vol. 6, p. 6-104.
[8] U. Credo, Diploma work, Meresburg, 1974, cited in *Landolt-Börstein, Numerical Data and Functional Relationships in Science and Technology*, New Series, edited by O. Madelung (Springer, New York, 1991), Group IV, Vol. 6, p. 6-104.
[9] D. P. Fernández, Y. Mulev, A. R. H. Goodwin, and J. M. H. Levelt-Sengers, J. Phys. Chem. Ref. Data **24**, 33 (1995).
[10] W. J. Ellison, K. Lamkaouchi, and J.-M. Moreau, J. Molecular Liquids **68**, 171 (1996).
[11] K. N. Marsh, Pure Appl. Chem. **53**, 1846 (1981).
[12] K. W. Wagner, Arch. Elektrotech. **3**, 100 (1914).